SIAM J. APPL. MATH.
Vol. 70, No. 8, pp. 3039–3064

STIMULUS-DRIVEN TRAVELING SOLUTIONS IN CONTINUUM NEURONAL MODELS WITH A GENERAL SMOOTH FIRING RATE FUNCTION*

G. BARD ERMENTROUT†, JOZSI Z. JALICS‡, AND JONATHAN E. RUBIN†

Abstract. We examine the existence of traveling wave solutions for a continuum neuronal network modeled by integro-differential equations. First, we consider a scalar field model with a general smooth firing rate function and a spatiotemporally varying stimulus. We prove that a traveling front solution that is locked to the stimulus exists for a certain interval of stimulus speeds. Next, we include a slow adaptation equation and obtain a formula, which involves a certain adjoint solution, for the stimulus speeds that induce locked traveling pulse solutions. Further, we use singular perturbation analysis to characterize an approximation to the adjoint solution that we compare to a numerically computed adjoint. Numerical simulations are used to illustrate the traveling fronts and pulses that we study and to make comparisons with our analytically computed bounds for stimulus-locked wave behavior.

Key words. waves, neuronal networks, integro-differential equations, neural field models

AMS subject classification. 92C20

DOI. 10.1137/090775737

1. Introduction.

Traveling waves in neural field models have been the subject of extensive mathematical investigation (reviewed in [9, 7]). The motive for the study of these waves comes from numerous experiments in brain slices. Putative roles for these waves are discussed in [10, 24]. Early work [5, 14] showed that it is possible to evoke propagation of traveling waves in brain slices that have been treated with drugs that block inhibition. Recently, experimentalists have become interested in the effects of heterogeneity and stimuli on these waves. For example, certain experiments examined the induction of traveling waves in cortical slices in which there were varying densities of cells [21, 6]. Reflections and blocking of these waves occur, as do changes in preferred directionality. Stimuli can have dramatic effects on waves. Xu et al. [26] show complex effects arising in visually evoked waves in rat cortex, and more recently, Takagaki et al. have shown that stimuli at two different locations can modulate the resulting waves (see [23, 25]). Richardson, Schiff, and Gluckmann [22] showed that electrical fields could be used to block, speed up, and slow down evoked waves.

Neural field models represent reductions and approximations of more "realistic" conductance-based models with the advantage of being much easier to analyze. Recently, the emergence of traveling waves, and other spatiotemporal patterns, was shown to occur in a neural field model to which a spatiotemporally varying stimulus was applied [2, 12, 13]. As in much of the work in this area, a Heaviside firing rate function was used in these papers. This simplification allows for the derivation of

*Received by the editors November 2, 2009; accepted for publication (in revised form) July 27, 2010; published electronically October 21, 2010.
http://www.siam.org/journals/siap/70-8/77573.html

†Department of Mathematics, University of Pittsburgh, Pittsburgh, PA 15260 (bard@math.pitt.edu, rubin@math.pitt.edu). The research of the first author was supported by NSF award DMS 0817131. The research of the third author was supported by NSF awards DMS 0716936 and DMS 1021701.

‡Department of Mathematics and Statistics, Youngstown State University, Youngstown, OH 44555 (jalics@math.ysu.edu). The research of this author was supported by NSF award DBI 0827205 and a YSU Research Professorship.

closed form solutions to the relevant field equations and analytical stability analysis, yet biologically, it implies that at each moment in time, cells either are firing at a unique nonzero constant rate or are not firing at all. The objective of this work is to study the effects of a spatiotemporally varying stimulus on a neural field model with a more realistic, smooth firing rate function. More specifically, we impose a small stimulus, $\varepsilon I(x,t)$, where $0 < \varepsilon \ll 1$ and $I(x,t) = I(x - ct)$ for some constant speed c, and we consider for what c values the field is able to follow the stimulus, in the sense that it supports a traveling wave solution of the same speed.

We analyze both a scalar field model and a model with adaptation. In the former case, our results build on the work of Ermentrout and McLeod [11], who proved the existence of monotone traveling fronts for a neural field without spatiotemporally varying stimulation, in one of the few rigorous works in this area allowing for a general smooth firing rate function (see also [18, 3, 19]). In the case with adaptation, we assume that the adaptation evolves slowly relative to the population firing rate and build on the singular perturbation construction of a traveling pulse solution done previously by Pinto and Ermentrout in the absence of spatiotemporally dependent applied stimulation [20].

2. Traveling fronts for a scalar field equation.

2.1. Existence. Consider a single-layer neuronal network model distributed over the real line with a small, spatiotemporally varying stimulus applied as follows:

$$\partial u(x,t)/\partial t = -u(x,t) + \int_{-\infty}^{\infty} J(x-y)F(u(y,t))\,dy + \varepsilon I(x,t). \tag{2.1}$$

Here, $u(x,t)$ denotes the mean membrane potential of a patch of tissue at position x and time t, $J(x)$ denotes the distance-dependent synaptic weight function that measures the strength of excitatory synaptic connections between neurons, $F(u)$ denotes the firing rate function that depends on the membrane potential u, and $\varepsilon I(x,t)$ denotes the small, spatiotemporally varying stimulus, where $0 < \varepsilon \ll 1$.

We consider the existence of a traveling front for (2.1) under the hypotheses on J, F given in [11].

(H1) The function $J(x)$ is defined, even, nonnegative, and absolutely continuous on $\mathbb{R}$, with $J' \in L^1(\mathbb{R})$ and $\int_{-\infty}^{\infty} J(x)\,dx = 1$.

(H2) The function $F(x)$ is defined and continuously differentiable on $[0,1]$, with $F' > 0$, $F'(0) < 1$, and $F'(1) < 1$. Moreover, the function $F(u) - u$ has precisely three zeros, at $u = 0,\ u = a$, and $u = 1$, with $0 < a < 1$.

To start, define the moving coordinate $\xi = x - ct$, and assume that the stimulus term I takes the form of a traveling front,

$$I(\xi) \to \begin{cases} 1, & \xi \to -\infty, \\ 0, & \xi \to \infty, \end{cases} \quad \text{and } I(\xi) \in (0,1) \text{ for all } \xi; \tag{2.2}$$

relevant $I(\xi)$ may be monotone decreasing, but assuming that this property holds is not necessary. We seek a traveling front solution $u(x - ct) = u(\xi)$ of (2.1) with the same speed c as the stimulus. Note that if $\varepsilon = 0$, or equivalently if $I \equiv 0$, then the results in [11] yield the existence of a family of monotone decreasing traveling fronts $u_0(\xi) = U(\xi - \theta)$, parametrized by $\theta \in \mathbb{R}$ (corresponding to translation), with $u_0(\xi) \to 1$ as $\xi \to -\infty$ and $u_0(\xi) \to 0$ as $\xi \to \infty$ for a special speed $c = c_0$. We assume that

(H3) $\int_0^1 (F(u)-u)\,du \neq 0$ such that $c_0 \neq 0$. The work in [11] can be used to establish the following result.

PROPOSITION 2.1. *For the solution u_0 of (2.1) with $\varepsilon = 0$, $u_0'(\xi) \in L^2(\mathbb{R})$.*

Proof. F and u_0 satisfy the equation ([11, p. 465])

$$-c_0 \int_{-\infty}^{\infty} (u_0')^2 F'(u_0)\,d\xi = \int_0^1 \{-u_0 + F(u_0)\}\,du_0,$$

so $\int_{-\infty}^{\infty}(u_0')^2 F'(u_0)\,d\xi$ takes a nonzero finite value, say i_0, by (H3). Moreover, by (H2), F' is strictly positive and continuous on $[0,1]$ such that it has a positive lower bound; call it m. Thus, $i_0 > 0$ and $\int_{-\infty}^{\infty}(u_0')^2\,d\xi \leq i_0/m < \infty$, as desired. ∎

To find traveling front solutions in the presence of the stimulus term $I(\xi)$, we rewrite (2.1) in a moving frame, up to first order in ε, as

$$-(c_0 + \varepsilon c_1)du/d\xi = -u + J(\xi) * F(u(\xi)) + \varepsilon I(\xi), \tag{2.3}$$

where $c = c_0 + \varepsilon c_1 + O(\varepsilon^2)$ and $u = u_0 + \varepsilon u_1 + O(\varepsilon^2)$. The following theorem characterizes traveling front solutions to (2.3).

THEOREM 2.2. *Let u_0 denote the nontrivial traveling front solution to (2.1), with $\varepsilon = 0$, and let c_0 be the corresponding wave speed. There is a unique nontrivial function $u^* \in L^2(\mathbb{R})$ that satisfies the adjoint equation*

$$\mathcal{L}^* u^* := (c_0 d/d\xi + 1)u^* - F'(u_0(\xi))(J(\xi) * u^*(\xi)) = 0 \tag{2.4}$$

together with the normalization condition

$$\int_{-\infty}^{\infty} u^*(\xi) u_0'(\xi)\,d\xi = 1.$$

Moreover, (2.3) has a solution $u_0(\xi) + \varepsilon u_1(\xi)$, with

$$u_1(\xi) \to \begin{cases} 0,\ \xi \to \infty, \\ (1 - F'(1))^{-1} \in (1,\infty),\ \xi \to -\infty, \end{cases} \tag{2.5}$$

if and only if $c_1 \in [0, C)$, where

$$0 < C := \sup_{\theta \in \mathbb{R}} \left(-\int_{-\infty}^{\infty} u^*(\xi - \theta) I(\xi)\,d\xi \right) \leq \bar{C} := -\int_{-\infty}^{\infty} u^*(\xi)\,d\xi. \tag{2.6}$$

Proof. At lowest order in ε, (2.3) is satisfied by $u_0(\xi - \theta)$ for any choice of θ. At first order, for fixed $\theta \in \mathbb{R}$, the equation for u_1 becomes

$$-c_0 u_{1_\xi}(\xi) + u_1(\xi) - J(\xi) * [F'(u_0(\xi - \theta))u_1(\xi)] = c_1 u_{0_\xi}(\xi - \theta) + I(\xi). \tag{2.7}$$

Rewrite the left-hand side of (2.7) as $\mathcal{L}u_1$ for $\mathcal{L} : L^2(\mathbb{R}) \to L^2(\mathbb{R})$. The operator $\mathcal{L}$ has $u_0'(\xi - \theta) < 0$ in its null space, based on differentiation with respect to ξ of the equation satisfied by u_0 and application of Proposition 2.1. Hence, by the Fredholm alternative, there exists $u^*(\xi - \theta)$, a nontrivial solution to the corresponding adjoint equation, $\mathcal{L}^* u = 0$, satisfying $u^* \in L^2(\mathbb{R})$.

Assuming that the solution u^* is sign-definite, it can be normalized such that

$$\int_{-\infty}^{\infty} u^*(\xi) u_0'(\xi)\,d\xi = 1, \tag{2.8}$$

and (2.7) has a solution if and only if

$$\langle u^*(\xi-\theta), c_1 u_{0_\xi}(\xi-\theta)+I(\xi)\rangle = 0. \tag{2.9}$$

Condition (2.9) is equivalent, based on the normalization (2.8) and the fact that $u_0(\xi)$ is monotone decreasing, to the condition

$$c_1 = -\int_{-\infty}^{\infty} u^*(\xi-\theta)I(\xi)\,d\xi \equiv S(\theta) > 0. \tag{2.10}$$

Thus, we expect to obtain a band of solutions, corresponding to c_1 values between the minimum and maximum values of $S(\theta)$. Based on the behavior of $I(\xi)$ assumed in (2.2), these values are 0 and $C \in (0, \bar{C}]$, as given in (2.6), respectively.

It remains to derive the adjoint equation (2.4) and to conclude that u^* is indeed sign-definite. If we write out the first order equation (2.7) in more detail, we see that

$$\langle \mathcal{L}u, v\rangle = \int_{-\infty}^{\infty} [(-c_0 d/d\xi+1)u(\xi)]v(\xi)\,d\xi - \int_{-\infty}^{\infty} v(\xi)\int_{-\infty}^{\infty} J(\xi-\eta)F'(u_0(\eta-\theta))u(\eta)\,d\eta\,d\xi.$$

If we apply integration by parts to the first integral and rewrite the second by Fubini's theorem, then we obtain

$$\langle \mathcal{L}u, v\rangle = \int_{-\infty}^{\infty} [(c_0 d/d\xi+1)v(\xi)]u(\xi)\,d\xi - \int_{-\infty}^{\infty} u(\eta)\left[F'(u_0(\eta-\theta))\int_{-\infty}^{\infty} J(\xi-\eta)v(\xi)\,d\xi\right]\,d\eta.$$

Hence, the relevant adjoint equation is

$$\mathcal{L}_\theta^* u^* := (c_0 d/d\xi+1)u^* - F'(u_0(\xi-\theta))(J(\xi) * u^*(\xi)) = 0.$$

Theorem 4.3 of [11] implies that for any fixed $\theta \in \mathbb{R}$, this equation has a solution that is unique, up to multiplication by a nonzero constant, and is sign-definite, which justifies the normalization (2.8). Finally, (2.5) follows from taking $\xi \to \pm\infty$ in (2.7) and noting that $u_{1_\xi}(\pm\infty) = u_{0_\xi}(\pm\infty) = u_0(\infty) = I(\infty) = 0$, $u_0(-\infty) = 1$, $I(-\infty) = 1$, and $F'(1) < 1$. ∎

Remark 2.3. Note that since u^* is sign-definite, the sign of c_1 is determined by the sign of the stimulus I. If I is replaced by $-I$, then the sign of c_1 switches, but its magnitude remains unchanged. Thus, the theory shows that application of small stimuli can speed up or slow down traveling fronts by equal amounts. We shall see that this is not the case when adaptation is included in the model in the next section.

In the next three subsections, we complement our analysis with some specific examples. In subsection 2.2, we consider the special case of a Heaviside firing rate function that, although it is not smooth, allows us to analytically compute the adjoint solution and thus to estimate the possible wave speeds as given by (2.10). Next, in subsection 2.3, we illustrate stimulus-locked front solutions of the original integral equation (2.1), computed numerically using a smooth firing rate function for appropriate stimulus wave speeds. Then, in subsection 2.4, we consider a special weight function that allows us to numerically approximate the bounds for possible stimulus-locked wave speeds given by (2.10) and compare them to the results obtained from direct simulations of (2.1).

2.2. A special case: Comparison to previous results. Although it does not have a derivative with a positive bound for $u \in [0,1]$, we formally consider the special case of a Heaviside firing rate, $F(u) = H(u-\sigma)$ for a threshold $\sigma \in (0,1)$, so

that we can compare Theorem 2.2 to previous results [13]. Without loss of generality, assume that $u_0(0) = \sigma$; that is, $\theta = 0$. In this case, the adjoint equation (2.4) formally becomes

$$c_0 w' + w = \delta(u_0(\xi) - \sigma) \int_{-\infty}^{\infty} J(\xi - \eta) w(\eta)\, d\eta. \tag{2.11}$$

To solve (2.11) for $w(\xi)$, use the integrating factor e^{ξ/c_0} and integrate to obtain

$$w(\xi) e^{\xi/c_0} = \frac{1}{c_0} \int_{-\infty}^{\xi} e^{\zeta/c_0} \delta(u_0(\zeta) - \sigma) \int_{-\infty}^{\infty} J(\zeta - \eta) w(\eta)\, d\eta\, d\zeta. \tag{2.12}$$

Since $\zeta \in (-\infty, \xi)$, it follows that $\delta(u_0(\zeta) - \sigma) \equiv 0$ for $\xi < 0$. Using this observation and switching the order of integration in (2.12) yields, for $\xi > 0$,

$$w(\xi) e^{\xi/c_0} = \frac{1}{c_0} \int_0^{\infty} \frac{J(\eta) w(\eta)}{|u_0'(0)|}\, d\eta \equiv B, \tag{2.13}$$

where B is a constant. That is, $w(\xi) = BH(\xi) e^{-\xi/c_0}$ for some constant B, where H as usual denotes the Heaviside step function.

To check the consistency of this solution, assume $\xi > 0$ and substitute it into both sides of (2.13) to obtain

$$B = \frac{B}{c_0} \int_0^{\infty} \frac{J(\eta) e^{-\eta/c_0}}{|u_0'(0)|}\, d\eta. \tag{2.14}$$

For consistency, the right-hand side of (2.14) should equal B. This is indeed the case for the choice $J(x) = e^{-|x|}/2$ since, using the corresponding calculation

$$u_0'(\xi) = -e^{-\xi}/(2(1 + c_0)) \tag{2.15}$$

from [11] or [13] evaluated at $\xi = 0$, we have

$$\frac{B}{c_0} \int_0^{\infty} \frac{J(\eta) e^{-\eta/c_0}}{|u_0'(0)|}\, d\eta = \frac{2B(1 + c_0)}{c_0} \int_0^{\infty} \frac{1}{2} e^{-\eta} e^{-\eta/c_0}\, d\eta = \frac{B(1 + c_0)}{c_0(1 + \frac{1}{c_0})} = B,$$

as desired. Note that this solution of (2.4), applied for arbitrary θ, yields

$$w(\xi - \theta) = BH(\xi - \theta) e^{-(\xi - \theta)/c_0}. \tag{2.16}$$

Now, to compute B, we use the normalization equation (2.8), with $u^* = w$ from (2.16) and $u_0'(\xi)$ from (2.15), to obtain

$$1 = B \int_0^{\infty} e^{-\xi/c_0} u_0'(\xi)\, d\xi = -B \int_0^{\infty} e^{-\xi/c_0} \frac{e^{-\xi}}{2(c_0 + 1)}\, d\xi.$$

After some calculation, we find $B = -2(1 + c_0)(\frac{1}{c_0} + 1)$.

Finally, the speed term c_1 is given by (2.10). To compare to the speed obtained previously for a stimulus with $O(\varepsilon)$ amplitude [13], take $I(\xi) = I_0 H(-\xi)$. Note that the lower bound for c_1 is 0, obtained from (2.10) for $\theta > 0$. For $\theta < 0$, (2.10) becomes

$$\begin{aligned} c_1 &= \textstyle\int_{-\infty}^{\infty} 2(1 + c_0)(\frac{1}{c_0} + 1) H(\xi - \theta) e^{-(\xi - \theta)/c_0} I_0 H(-\xi)\, d\xi \\ &= 2I_0(1 + c_0)(\tfrac{1}{c_0} + 1) \textstyle\int_{\theta}^{0} e^{-(\xi - \theta)/c_0}\, d\xi. \end{aligned} \tag{2.17}$$

Using the fact that $c_0 = (1-2\sigma)/(2\sigma)$ from [11], evaluation of this integral and some algebra yield

$$c_1 = \frac{I_0(1-e^{\theta/c_0})}{2\sigma^2}. \tag{2.18}$$

Thus, the upper bound for c_1 is $\frac{I_0}{2\sigma^2}$, which is approached as $\theta \to -\infty$. According to [13], the right boundary of the existence region in the (c, I_0)-plane is given by $c = \frac{1}{2(\sigma - \varepsilon I_0)} - 1$. Note that this speed is approached as $\xi_0 \to -\infty$. Rewriting this expression for c as $c_0 + \varepsilon c_1$ with $c_0 = \frac{1}{2\sigma} - 1$ and solving for c_1 results in

$$c_1 = \frac{I_0}{2\sigma(\sigma - \varepsilon I_0)} = \frac{I_0}{2\sigma^2} + O(\varepsilon). \tag{2.19}$$

Consequently, our existence regions agree within $O(\varepsilon)$ to those of [13]; that is, for both techniques, $c \in [c_0 = \frac{1}{2\sigma} - 1, c_0 + \varepsilon(\frac{I_0}{2\sigma^2} + g(\sigma, I_0, \varepsilon)))$, where $g(\sigma, I_0, \varepsilon) = O(\varepsilon)$ and $0 < \sigma \leq 1/2$.

2.3. Numerical simulations of the front. In this subsection, we present typical numerical simulations of (2.1). These results show examples of the successful propagation of traveling fronts that track moving stimuli as well as examples of failures to track. Of course, it is not possible to simulate (2.1) on the whole real line in space or time. For each example, we consider the domain $x \in [-1, 1]$ with even boundary conditions, and we choose a stimulus function $I(\xi)$ and a relevant initial condition $u(x, 0)$ for $x \in [-1, 1]$. In some cases, we assume that the stimulus function $I(\xi)$ is the Heaviside step function $H(-\xi - b)$ for some choice of $b \in (0, 1)$ and $c > 0$, with $\xi = x - ct$, such that (2.2) is satisfied. To approximate the arrival of a traveling front solution of (2.1) to a particular interval of x values within a larger (e.g., infinite) spatial domain, we simulate with initial conditions $u(x, 0) > 0$ for x near -1 and $u(x, 0) = 0$ for all other $x \in [-1, 1]$. We predict that, for this initial configuration with stimulus $\varepsilon I(\xi)$ applied for small $\varepsilon > 0$, we will observe activity propagating in the direction of increasing x with speed c, the speed of the stimulus, if and only if c is sufficiently close to the interval $[c_0, c_0 + \varepsilon C)$, where C is given by (2.6). Similarly, we also consider stimuli $-\varepsilon I(\xi) = -\varepsilon H(-\xi - b)$ to follow up on Remark 2.3, and we expect to observe propagation on $(c_0 - \varepsilon C, c_0]$ in this case.

For our simulations, we use $F(u) = 1/(1 + \exp(-20u + 5))$ and $J(x) = 10\exp(-20|x|)$ and normalize the natural, unstimulated wave speed to $c_0 = 1$. Consider first a simulation in which we start with u activated in the leftmost 5% of the domain by using initial conditions $u(x, 0) = 0.9H(-x - 0.9)$ and with the front of the stimulus, which will move with speed c, slightly ahead of the activated region, choosing $b = 0.8$ such that $I(x, 0) = H(-x - 0.8)$. We find that for a stimulus magnitude of $\varepsilon = 0.01$, the interval of speeds for which stimulus-locked traveling fronts exist is roughly $c \in [1, 1.2)$. For a stimulus speed of $c = 1.1$, for example, the front that is initiated by the initial conditions succeeds in tracking closely behind the stimulus and propagating from left to right with the same speed as the stimulus front. This is illustrated in Figure 1(a), where we plot $u(x, t) + 10\varepsilon I(x, t)$ to show the close tracking of the wave front to the stimulus front. With all the same conditions and a faster stimulus speed of $c = 1.3$, the simulated wave front fails to keep up with the faster stimulus front, falling farther and farther behind as seen in Figure 1(b).

Next, we consider the case of a negative (inhibitory) stimulus of the same magnitude. That is, we replace $\varepsilon I(x, t)$ with $-\varepsilon I(x, t)$ and keep all other conditions the

same, and we find that the existence interval for stimulus-locked traveling fronts is roughly $c \in [0.8, 1)$. This is consistent with our analysis that shows that two stimuli of the same magnitude but opposite sign can speed up or slow down traveling fronts by the same amount (see Remark 2.3). A successful stimulus-locked traveling front is shown in Figure 1(c) for $c = 0.9$; whereas a failure to track is shown in Figure 1(d)

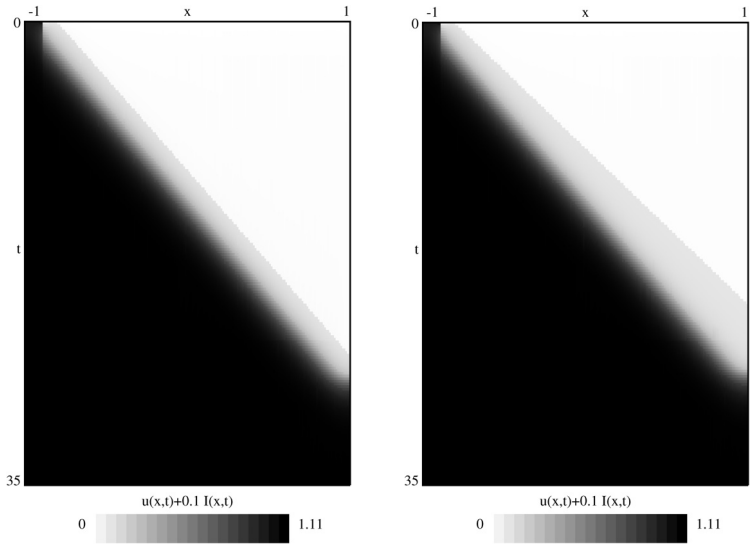

(a) c=1.1

(b) c=1.3

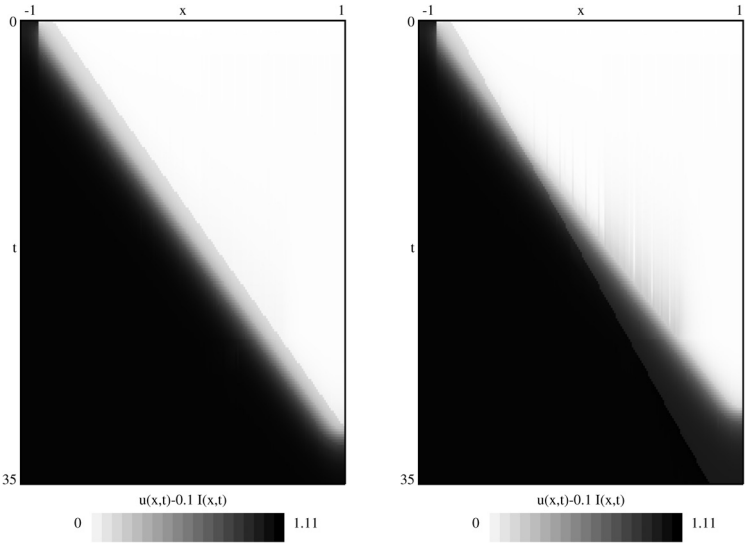

(c) c=0.9

(d) c=0.7

FIG. 1. *Stimulus-locked traveling fronts.* (a), (c) *Successful and* (b), (d) *failed propagation with* (a), (b) $\varepsilon I(x,t) = 0.01H(-(x-ct)-0.8)$ *and* (c), (d) $\varepsilon I(x,t) = -0.01H(-(x-ct)-0.8)$. *For these simulations,* $F(u) = 1/(1+\exp(-20u+5))$ *and* $J(x) = 10\exp(-20|x|)$.

with $c = 0.7$, where $u(x,t) - 10\varepsilon I(x,t)$ is plotted in each case to show the relation of the traveling front to the stimulus front. We note that the successful, stimulus-locked fronts in Figure 1(a) and (c) correspond to the analytically computed traveling fronts. However, the frontlike solutions in Figure 1(b) and (d) that do not lock to the stimulus do not represent true traveling wave solutions on the entire real line but rather provide evidence that traveling wave solutions do not exist for those values of c outside of the existence interval.

Remark 2.4. The particular interval of speeds c for which stimulus-induced wave propagation succeeds depends on the form of $I(\xi)$, in addition to its amplitude, as indicated in (2.6). For example, suppose we replace the Heaviside stimulus with a monotone increasing sigmoidal stimulus $I(\xi) = 1/(1 + \exp((-\xi - b)/\rho))$, $\rho > 0$. Successful stimulus tracking occurs on progressively larger intervals of c as ρ increases. Tracking does not seem to be particularly sensitive to the precise value selected for b.

Remark 2.5. We have investigated the effect of varying the sigmoidal firing rate function of the form $F(u) = 1/(1+\exp(-Au+B))$. Our simulations focus on firing rate functions consistent with hypothesis (H2) from subsection 2.1 of our analysis. Namely, we focus on choices of A and B such that $F(u)-u$ has zeros near 0 and 1 and at a where $0 < a < 0.5$. The baseline case shown in Figure 1(a)–(d) has $A = 20, B = 5, a \approx 0.17$, and $c_0 \approx 1.3$, with successful tracking for the given positive and negative stimuli to within about 10% of the normalized natural wave speed. For different choices of A, B such that $0 < a < 0.5$ (e.g., $A = 10,\ B = 4,\ a \approx 0.33,\ c_0 \approx 0.44$; $A = 40,\ B = 10,\ a \approx 0.22,\ c_0 \approx 1.05$; $A = 7,\ B = 3,\ a \approx 0.32,\ c_0 \approx 0.47$), we find that successful tracking occurs to within about 10% of the normalized natural wave speed as in the baseline case. Thus, it appears that varying the shape of the sigmoidal firing rate function changes the absolute range of speeds for which stimulus-locked fronts exist, but the relative range of possible speeds remains approximately the same. For choices of A, B such that $F(u)-u$ has no zeros (e.g., A=10, B=6), no natural waves exist, but stimuli of very large amplitude (e.g., 0.3) are able to induce stimulus-locked fronts. An analysis of this scenario is beyond the scope of this paper since we are interested in relatively weak stimuli that harness the natural wave-generating capability of the medium rather than imposing a wave on the medium through application of a large stimulus.

2.4. Numerical approximations of the front speed. In this subsection, we use (2.10) and a numerical computation of the adjoint to approximate possible stimulus-locked front speeds. We consider the special weight function

$$J(x) = \frac{1}{2}e^{-|x|}, \tag{2.20}$$

as this will enable us to reduce the computation of the front and the adjoint to an ODE shooting problem. We recall that the integral equation for the natural wave ((2.3) with $\varepsilon = 0$) is

$$-c_0 u' = -u + \int_{-\infty}^{\infty} J(\xi - \eta)F(u(\eta))\ d\eta, \tag{2.21}$$

and, given $u(\xi)$, the corresponding adjoint equation is

$$c_0(u^*)' = -u^* + F'(u(\xi)) \int_{-\infty}^{\infty} J(\xi - \eta)u^*(\eta)\ d\eta.$$

We let

$$w(\xi) = \int_{-\infty}^{\infty} J(\xi - \eta) F(u(\eta))\ d\eta = J * F(u)$$

such that application of the Fourier transform yields $\hat{w}(k) = [\hat{F}(u)](k)/(1+k^2)$. In this case, $[\hat{F}(u)](k) = (1+k^2)\hat{w}(k)$ such that inversion of the Fourier transform gives $w - w'' = F(u)$. Thus, establishing the existence of an unstimulated front is reduced to solving

$$\begin{aligned} -c_0 u' &= -u + w, \\ w' &= z, \\ z' &= w - F(u), \end{aligned} \tag{2.22}$$

and finding a heteroclinic orbit from $(u, w, z) \approx (1, 1, 0)$ to $(u, w, z) \approx (0, 0, 0)$. We solve this equation numerically via shooting, taking advantage of the one-dimensional stable manifold at $(u, w, z) \approx (0, 0, 0)$.

Similarly, we let

$$p(\xi) = \int_{-\infty}^{\infty} J(\xi - \eta) u^*(\eta)\ d\eta$$

to obtain an ODE for the adjoint

$$\begin{aligned} c(u^*)' &= -u^* + F'(u(\xi))p, \\ p' &= r, \\ r' &= p - u^*. \end{aligned} \tag{2.23}$$

The adjoint solution we seek corresponds to a homoclinic solution asymptotic to $(u^*, p, r) = (0, 0, 0)$ that satisfies the normalization condition $\int_{-\infty}^{\infty} u'(\xi) u^*(\xi)\ d\xi = 1$, which we obtain through a proper choice of initial conditions for (2.23). For specific simulations, we use $F(u) = 1/(1+\exp(-20u+5))$. With these parameters, integration of the discretized integral equation (2.21) yields $c_0 = 1.29158$ while the shooting method gives us $c_0 = 1.2941$. We display the solutions $u(\xi)$, $u'(\xi)$, and $u^*(\xi)$ from (2.22) and (2.23) in Figure 2(A).

With this calculation of $u^*(\xi)$, we can compute the range of values of c such that we can lock to the stimulus, $I(\xi)$. Recall that $c = c_0 + \varepsilon c_1$ is, up to $O(\varepsilon)$, the velocity of the stimulus, with tracking predicted for $c_1 = -\int_{-\infty}^{\infty} u^*(\xi - \theta) I(\xi) d\xi := S(\theta)$ for some θ. For the step-function stimulus, $I(\xi) = \mathrm{H}(-\xi)$, we compute $S(\theta)$ and illustrate it in Figure 2(B). From the figure, it can be seen that there is an upper bound to the velocity that can be followed, and that with positive stimuli only, velocities faster than c_0 can be followed. Furthermore, since S is effectively nonzero only when $\theta > 0$, this means that the front will always lag the stimulus by some amount.

In Figure 2(C) and (D), we show the results of a simulation of the full integral equation (as in subsection 2.3) with a stimulus of amplitude $I_0 = 0.01$ moving at velocities of $c = c_0 + \Delta c$ with Δc plotted along the x-axis. Figure 2(C) shows that the time difference (lag) Δt between the stimulus front and the wave front is an increasing function of Δc, consistent with Figure 2(B). The two curves correspond to two different spatial locations. The fact that there is not perfect overlap is likely due to the slow speed of convergence of the wave to the stimulus (which should be $O(1/\varepsilon)$). We can also quantitatively compare the simulation results in Figure 2(C) with the

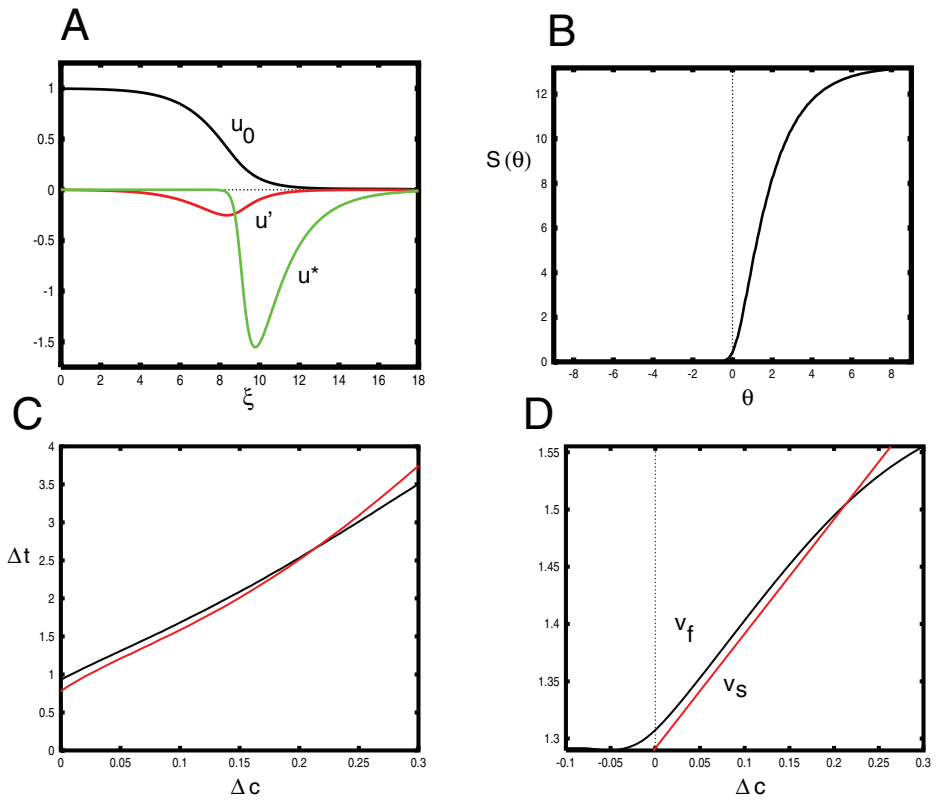

FIG. 2. (A) *Numerical simulations of* $u(\xi), u'(\xi)$, *and* $u^*(\xi)$ *from* (2.22)–(2.23). (B) *Numerical calculation of* $S(\theta)$ *using* $u^*(\xi)$ *from* (A) *and* (2.10). (C) *Plots of time difference (lag)* Δt *between the stimulus front and the wave front versus* Δc *at two different spatial locations.* (D) *Plots of the velocities of the front* (v_f) *and stimulus* (v_s) *versus* Δc, *suggesting that stimulus-locking behavior will occur with the bounds of* $\Delta c = 0$ *and* $\Delta c \approx 0.15$.

results from Figure 2(B). For example, if we take $\Delta c = 0.05$, then since the magnitude of the stimulus is 0.01, this corresponds to $c_1 = 5$. We read from Figure 2(B) that $S(\theta) = 5$ for $\theta \approx 1.5$. Since the natural wave velocity is approximately 1.3, we would expect a time difference between the leading edge of the stimulus and the front to be about $1.5/1.3 = 1.15$; whereas Figure 2(C) gives a similar value of about 1.2–1.3.

In Figure 2(D) we plot the velocities of the front (v_f) and stimulus (v_s) versus Δc to explore the limits of the stimulus-locking behavior. It is difficult to determine precisely the limits of locking behavior from Figure 2(D), but we estimate, based on where the curves start to become nonparallel, that the wave can be followed up to about $\Delta c = 0.15$, which is consistent with the simulations shown in Figure 1. Since the maximum of $S(\theta)$ from Figure 2(B) is about 13 and $I_0 = 0.01$, our analysis yields an estimate of 0.13 as the upper bound on speeds that can be followed. We might get even better estimates for smaller I_0; however, the comparison would become very difficult in that case, since the small values of Δc would take very long spatial distances to resolve.

3. Traveling pulses with slow adaptation. We now include a slow adaptation equation in the neural field model under consideration and seek to extend an

earlier singular perturbation construction of a pulse solution [20] to allow for the inclusion of a small, spatiotemporally pulsatile stimulus. Unlike the analysis in subsection 2.1, our approach here is not fully rigorous. In particular, we do not have sufficient information about the derivative of the pulse solution to draw rigorous conclusions about the existence and uniqueness of a solution to a relevant adjoint equation. We will nonetheless proceed formally to derive a formula for the stimulus speeds for which traveling pulses are predicted to exist. Furthermore, for numerical experimentation and more precise estimation of the stimulus speeds that can be tracked, we will consider solutions with the particular weight function $J(x) = \frac{1}{2}e^{-|x|}$ and approximate the homoclinic solution corresponding to the pulse solution with a large amplitude periodic solution.

With adaptation, the model equations that we consider become

$$\begin{aligned} \partial u(x,t)/\partial t &= -u(x,t) + \textstyle\int_{-\infty}^{\infty} J(x-y)F(u(y,t))\,dy - q(x,t) + \varepsilon I_a(x,t), \\ \partial q(x,t)/\partial t &= \kappa(-\beta q(x,t) + u(x,t)), \end{aligned} \tag{3.1}$$

where $0 < \kappa \ll 1$, $0 < \varepsilon \ll 1$, and $q(x,t)$ represents a negative feedback recovery mechanism such as spike frequency adaptation. We introduce the moving coordinate $\xi = x - ct$ and assume a pulsatile stimulus with $I_a(x,t) = I_a(\xi) \to 0$ as $\xi \to \pm\infty$. We seek traveling pulse solutions that are locked to the stimulus. Using our earlier notation for convolutions, traveling pulse solutions to (3.1) satisfy

$$\begin{aligned} -cu'(\xi) &= -u(\xi) + J * F(u(\xi)) - q(\xi) + \varepsilon I_a(\xi), \\ -cq'(\xi) &= \kappa(u(\xi) - \beta q(\xi)), \end{aligned} \tag{3.2}$$

together with the boundary conditions $(u,q)(\xi) \to 0$ as $\xi \to \pm\infty$.

3.1. Fredholm alternative gives expression for relevant wave speeds. Write $c = c_0 + \varepsilon c_1$, $u = u_0 + \varepsilon u_1$, $q = q_0 + \varepsilon q_1$ to leading order in the small parameter ε, with

$$u_1, q_1 \to 0 \text{ as } \xi \to \pm\infty. \tag{3.3}$$

With this notation, system (3.2) becomes

$$\begin{aligned} -(c_0 + \varepsilon c_1)(u_{0_\xi} + \varepsilon u_{1_\xi}) &= -(u_0 + \varepsilon u_1) + J * F(u_0 + \varepsilon u_1) - (q_0 + \varepsilon q_1) + \varepsilon I_a, \\ -(c_0 + \varepsilon c_1)(q_{0_\xi} + \varepsilon q_{1_\xi}) &= \kappa[(u_0 + \varepsilon u_1) - \beta(q_0 + \varepsilon q_1)]. \end{aligned} \tag{3.4}$$

We take as a given the existence of a pulse $(u_0(\xi), q_0(\xi))$ in the unstimulated case with $\varepsilon = 0$, as was shown analytically to exist in the $\kappa \downarrow 0$ singular limit in [20], and we solve for the $O(\varepsilon)$ correction terms introduced by the stimulus. At $O(\varepsilon)$, we find

$$\begin{aligned} -c_1 u_{0_\xi} - c_0 u_{1_\xi} &= -u_1 + J * F'(u_0)u_1 - q_1 + I_a, \\ -(c_1 q_{0_\xi} + c_0 q_{1_\xi}) &= \kappa(u_1 - \beta q_1). \end{aligned} \tag{3.5}$$

Rewrite (3.5) as

$$\begin{aligned} \mathcal{L}_a \begin{pmatrix} u_1 \\ q_1 \end{pmatrix} := \begin{pmatrix} -c_0 u_1' + u_1 - J(\xi) * F'(u_0)u_1 + q_1 \\ -c_0 q_1' - \kappa u_1 + \kappa\beta q_1 \end{pmatrix} &= \begin{pmatrix} c_1 u_0' + I_a \\ c_1 q_0' \end{pmatrix} \\ &= \begin{pmatrix} I_a \\ 0 \end{pmatrix} + c_1 \begin{pmatrix} u_0' \\ q_0' \end{pmatrix}. \end{aligned} \tag{3.6}$$

Let $(u^*(\xi-\theta), q^*(\xi-\theta))$ denote any solution to the adjoint equation $\mathcal{L}_a^*\binom{u^*}{q^*} = 0$, parametrized by $\theta \in \mathbb{R}$, corresponding to translation invariance of traveling wave solutions of (3.1). According to the Fredholm alternative, system (3.6) has a nontrivial solution if and only if for some such (u^*, q^*),

$$\int_{-\infty}^{\infty} c_1(u_0'(\xi-\theta)u^*(\xi-\theta) + q_0'(\xi-\theta)q^*(\xi-\theta))d\xi + \int_{-\infty}^{\infty} I_a(\xi)u^*(\xi-\theta)d\xi = 0. \tag{3.7}$$

Normalizing such that

$$\int_{-\infty}^{\infty} (u_0'(\xi-\theta)u^*(\xi-\theta) + q_0'(\xi-\theta)q^*(\xi-\theta))d\xi = 1 \tag{3.8}$$

yields the result that traveling pulses exist for speeds $c = c_0 + \varepsilon c_1 + O(\varepsilon^2)$, where

$$c_1 = -\int_{-\infty}^{\infty} u^*(\xi-\theta)I_a(\xi)d\xi \equiv S(\theta). \tag{3.9}$$

Thus, we expect to obtain a band of solutions, corresponding to c_1 values between the minimum and maximum values of $S(\theta)$, i.e., for $c_1 \in [C_m, C_M]$, where

(3.10)

$$C_m := \inf_{\theta\in\mathbb{R}} \left(-\int_{-\infty}^{\infty} u^*(\xi-\theta)I_a(\xi)\,d\xi \right) < c_1 < \sup_{\theta\in\mathbb{R}} \left(-\int_{-\infty}^{\infty} u^*(\xi-\theta)I_a(\xi)\,d\xi \right) := C_M.$$

Remark 3.1. In subsection 3.2, we approximate the traveling pulse by a singular periodic orbit consisting of segments along a slow manifold and fast jumps between these segments. The adjoint solution corresponding to this periodic orbit is unique up to constant multiplication, suggesting that the nontrivial solution (u^*, q^*) of $\mathcal{L}_a^*\binom{u^*}{q^*} = 0$, appearing in (3.8) and (3.9), is unique as well.

Remark 3.2. Our subsequent calculations, in subsection 3.2, and numerical simulations, in subsection 3.3, illustrate that u^* need not be sign-definite, unlike the case of traveling fronts without adaptation. Hence, in the presence of a particular stimulus, waves may exist for an interval of speeds that is not symmetric about the unstimulated speed c_0. Moreover, (3.9) and (3.10) suggest that when a stimulus is replaced with one of opposite sign but equal amplitude, the existence interval for stimulus-locked pulses can be obtained by a reflection about the natural wave speed. For example, an existence interval of the form $(c_0 - a, c_0 + b)$ with $a, b > 0$ for a stimulus εI_a suggests an existence interval of the form $(c_0 - b, c_0 + a)$ for a stimulus $-\varepsilon I_a$.

3.2. Behavior of the solution to the adjoint equation. To gain more information about our estimate of c_1, given by (3.9), we seek to characterize the behavior of nontrivial solutions (u^*, q^*) to the adjoint equation corresponding to (3.6). To do so, it is convenient to approximate the traveling pulse solution by a periodic orbit of large period so that we can use certain theoretical results obtained for adjoint solutions to such periodic solutions. Previous work has established that the singular perturbation construction of traveling pulses to a reaction-diffusion analogue of (3.1) on the real line, in the absence of stimulation, generalizes directly to give the existence of a periodic solution on a finite spatial domain with periodic boundary conditions [4]. Indeed, the argument for the existence of traveling pulses in [20] shows how to generalize the construction in [4] to the unstimulated form of (3.1), and the extension to the periodic case follows immediately.

Let $w = J * F(u)$, the convolution term from system (3.1). As in subsection 2.4, we will consider the special case of

$$J(x) = \frac{1}{2}e^{-|x|} \tag{3.11}$$

such that application of the Fourier transform yields $\hat{w}(k) = [\hat{F}(u)](k)/(1+k^2)$. Recall that this case gives $[\hat{F}(u)](k) = (1+k^2)\hat{w}(k)$ such that inversion of the Fourier transform yields $F(u) = w - w''$ for $' = d/d\xi$. With this notation in place, traveling pulse solutions to the unstimulated form of (3.1), namely, solutions to (3.2) with $\varepsilon = 0$, correspond to homoclinic solutions of

$$\begin{aligned} -cu' &= -u + w - q, \\ -cq' &= \kappa(u - \beta q), \\ w' &= z, \\ z' &= w - F(u), \end{aligned} \tag{3.12}$$

with $0 < \kappa \ll 1$. We seek periodic solutions of this system that approximate the homoclinic solution. An example of such a solution, computed numerically and projected into (u, q)-space, is shown in Figure 3(a). To find this periodic orbit, we used shooting with time reversed, because the spectrum of the linearization of the system features three positive eigenvalues and one negative eigenvalue in forward time. These become one positive and three negative eigenvalues in reversed time, rendering the shooting problem more tractable. Two additional periodic orbits, computed similarly but with longer periods, are shown in Figure 3(b). Note that these orbits extend closer to the projection of the critical point of (3.12) with increasing period, supporting the validity of the periodic approximation to the homoclinic solution.

To move forward analytically, we will use the fast subsystem defined from (3.12) by setting $\kappa = 0$, which consists of the u, w, z equations from (3.12) together with

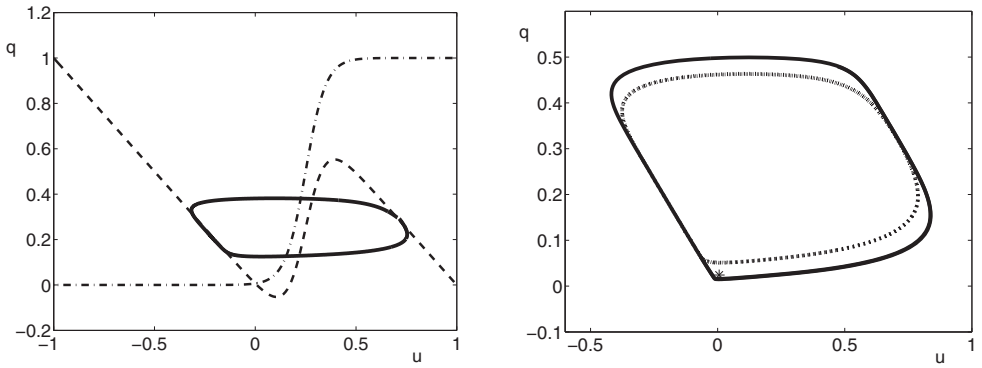

(a) (b)

FIG. 3. *Numerically estimated periodic solutions of* (3.12)*, projected to the* (u, q)*-plane.* (a) *Periodic solution (solid), slow manifold* $\mathcal{S}$ *(dashed), and graph of* $(u, F(u))$ *(dash-dotted). Here,* $c = 0.38, \kappa = 0.02, \beta = 0.25, F(u) = 1/(1 + \exp(-20u + 5))$*. The flow along the periodic orbit with respect to* ξ *or* ζ *is clockwise.* (b) *Periodic orbits of higher periods approach closer to the projection of the critical point of* (3.12)*, with* $u \approx 0.06$ *and* $q \approx 0.024$*, as marked with an asterisk.*

$q' = 0$ such that q is constant. We will also use the slow formulation of system (3.12), given by

$$\begin{aligned} -c\kappa \dot{u} &= -u + w - q, \\ -c\dot{q} &= u - \beta q, \\ \kappa \dot{w} &= z, \\ \kappa \dot{z} &= w - F(u), \end{aligned} \tag{3.13}$$

where differentiation is with respect to $\zeta = \kappa\xi$. The singular slow flow for this system is given by setting $\kappa = 0$ in (3.13) to obtain

$$-c\dot{q} = u - \beta q. \tag{3.14}$$

This flow is relevant on the slow manifold $\mathcal{S}$ defined by $u - w + q = 0, z = 0, w = F(u)$ or, equivalently, $\{(u, q, w, z) : z = 0, q = F(u) - u\}$, in the $\kappa \to 0$ limit. Projected to (u, q)-space, $\mathcal{S}$ takes the form of the dashed curve shown in Figure 3(a). Note that the flow along the periodic with respect to ξ or ζ is clockwise, given that $d/d\zeta = (-1/c\kappa)(d/dt)$, if we consider the case $c > 0$.

Before we proceed further, we make two important observations. First, note that the adjoint system to (3.12), reordered to put the slow q equation last, is

$$(x^*)' = M^* x^*, \tag{3.15}$$

where $x^* = [u^* \;\; w^* \;\; z^* \;\; q^*]^T$ and

$$M^* = \begin{bmatrix} -1/c & 0 & F'(u) & \kappa/c \\ 1/c & 0 & -1 & 0 \\ 0 & -1 & 0 & 0 \\ -1/c & 0 & 0 & -\beta\kappa/c \end{bmatrix}. \tag{3.16}$$

If we instead directly consider the equation $\mathcal{L}_a \binom{u}{q} = 0$, with $\mathcal{L}_a$ from (3.6), then the corresponding adjoint equations are

$$\begin{aligned} (u^*)' &= (F'(u)J * u^* - u^* + \kappa q^*)/c, \\ (q^*)' &= (-u^* - \kappa\beta q^*)/c. \end{aligned}$$

Now, let $z^* = (J * u^*)/c$. Using the form of J given in (3.11), the Fourier transform yields $\hat{u}^*(k) = c(1 + k^2)\hat{z}^*(k)$ such that $u^*/c = z^* - (z^*)''$. Finally, if we set $w^* = -(z^*)'$, then we recover the adjoint system (3.15) and (3.16). Thus, the (u^*, q^*) components to solutions to the adjoint equations for system (3.12) satisfy the adjoint equation $\mathcal{L}_a^* \binom{u^*}{q^*} = 0$ that is relevant for speed estimation through (3.8) and (3.9) and vice versa.

By construction, solutions of (3.2) with $\varepsilon = 0$ satisfy system (3.12). The second observation that we make here is that all solutions to (3.12) also satisfy (3.2) with $\varepsilon = 0$. This can be seen by direct solution of the equation $w'' - w = -F(u)$ with variation of parameters. Indeed, when done on the real line, for example, this calculation yields $w(\xi) = \frac{1}{2}\int_{-\infty}^{\infty} F(u(\xi))e^{-|\eta-\xi|}\, d\eta = J * F(u)$, as desired.

Next, we would like to apply Theorem A.1 from [15] to characterize the limit to which the solution $(u^*(\zeta), q^*(\zeta), w^*(\zeta), z^*(\zeta))$ to the adjoint equations (3.15) and

(3.16), expressed with respect to the slow time $\zeta = \kappa\xi$, tends as the singular perturbation parameter $\kappa \downarrow 0$. As it is stated, this theorem applies to a relaxation oscillation solution that, in the singular limit, makes fast jumps from the knees of an underlying cubic-shaped slow manifold. The theorem provides explicit formulas for the jumps in the components of the adjoint solution that occur when the underlying relaxation oscillation jumps up and down. These formulas depend on the direction tangent to which the jumps originate. This direction is given by a left eigenvector of the Jacobian matrix of a fast subsystem, corresponding to the eigenvalue $\lambda = 0$ that exists precisely at the knees. In our notation, the knees are those points on $\mathcal{S}$ such that $F'(u) = 1$. However, since we consider a traveling pulse solution, the relevant jumps do not occur where $F'(u) = 1$. Nonetheless, we can easily generalize the theorem and its formulas by picking out the tangent eigenvector to the jump directions. Further details of the relevant calculations are given in the appendix.

Let $u = g_\alpha(q)$ denote the solutions to $q = F(u) - u$ on the left branch of $\mathcal{S}$, with $\alpha = L$, and on the right branch of $\mathcal{S}$, with $\alpha = R$. Implicit differentiation on $\mathcal{S}$ yields

$$1 = (F'(g_\alpha(q)) - 1)g'_\alpha(q). \tag{3.17}$$

On $\mathcal{S}$, the slow flow (3.14) becomes

$$\dot{q} = (\beta q - g_\alpha(q))/c.$$

Moreover, from the slow formulation of (3.15) and (3.16) in the $\kappa \to 0$ limit and equation (3.17), it follows that the corresponding slow adjoint equation is

$$\dot{q}^* = -(\beta/c)q^* + (1/c)g'_\alpha(q)q^*, \tag{3.18}$$

with corresponding normalization condition [15]

$$q^*(\beta q - g_\alpha(q))/c = 1. \tag{3.19}$$

Assume that a periodic orbit of system (3.13) has period ζ_p, let $\zeta_1 < \zeta_2 \in (0, \zeta_p)$ denote the two jump times associated with the orbit, and suppose that each jump takes off from a point a_j and lands at a point b_j. For any function f, let $f(\zeta_j^-) = \lim_{\zeta \uparrow \zeta_j} f(\zeta)$ and $f(\zeta_j^+) = \lim_{\zeta \downarrow \zeta_j} f(\zeta)$. The generalization of Theorem A.1 of [15] implies (see the appendix) that

$$q^*(\zeta_j^+) = q^*(\zeta_j^-) - c\left(\frac{G(b_j) - G(a_j)}{G(a_j)G(b_j)}\right), \qquad j = 1, 2, \tag{3.20}$$

where $G(x) = (\beta q - g_\alpha(q))|_{(u,q,w,z)=x}$. Moreover,

$$\begin{bmatrix} u^* \\ w^* \\ z^* \end{bmatrix}(\zeta) = \begin{bmatrix} 1/(1 - F'(u)) \\ 0 \\ 1/(c(1 - F'(u))) \end{bmatrix} q^*(\zeta) + \begin{bmatrix} c^2 \\ c\lambda/(1 - \lambda^2) \\ c/(1 - \lambda^2) \end{bmatrix} \left(\frac{G(b_j) - G(a_j)}{G(a_j)G(b_j)}\right) \delta(\zeta - \zeta_j), \tag{3.21}$$

where λ is a certain eigenvalue of the Jacobian matrix of the fast subsystem of (3.12). Since we are not concerned with the jumps in w^*, z^*, we do not give an explicit formula for λ. Importantly, our original hypothesis that $F' > 0$, within (H2), implies that $\lambda \neq 1$; see the appendix for further details.

Remark 3.3. A transversality assumption is made in Theorem A.1 of [15] that here amounts to $\lambda \neq 1$. In fact, we shall see in the appendix that $\lambda \neq 1$ is guaranteed by our assumption that $F'(u) \neq 0$.

At the jump up of the periodic solution,

$$\frac{G(b_1)-G(a_1)}{G(a_1)G(b_1)} = \frac{g_L(q(\zeta_1))-g_R(q(\zeta_1))}{(\beta q(\zeta_1)-g_L(q(\zeta_1)))(\beta q(\zeta_1)-g_R(q(\zeta_1)))} > 0, \tag{3.22}$$

which yields $q^*(\zeta_1^+) < q^*(\zeta_1^-)$ from (3.20). At the jump down,

$$\frac{G(b_2)-G(a_2)}{G(a_2)G(b_2)} = \frac{g_R(q(\zeta_2))-g_L(q(\zeta_2))}{(\beta q(\zeta_2)-g_R(q(\zeta_2)))(\beta q(\zeta_2)-g_L(q(\zeta_2)))} < 0, \tag{3.23}$$

which yields $q^*(\zeta_2^+) > q^*(\zeta_2^-)$. Between these jumps, q^* experiences an exponential ζ-dependence, as specified by (3.18). The magnitudes and signs of the jumps in u^*, namely, $u^*(\zeta_i^+) - u^*(\zeta_i^-)$ for $i = 1, 2$, will depend on the comparison of $F'(u(\zeta_i^+))$ with $F'(u(\zeta_i^-))$, as specified in (3.21). Interestingly, it can also be seen from (3.21), (3.22), and (3.23) that in the singular limit, the signs of the δ-function excursions of u^* at the two jumps will be in opposite directions to each other, and each will be in the opposite direction to the corresponding jump of q^*.

We can get additional insight from the periodic orbit shown in Figure 3(a). In this example, the take-offs and landings of both jumps occur from points where $F'(u) \approx 0$. Hence, we expect that each jump in u^* will be of a very similar magnitude to that in q^*, since (3.21) implies that

$$\begin{aligned} u^*(\zeta_i^+) - u^*(\zeta_i^-) &= \left(\frac{1}{1-F'(u(\zeta_i^+))}\right) q^*(\zeta_i^+) \\ &\quad - \left(\frac{1}{1-F'(u(\zeta_i^-))}\right) q^*(\zeta_i^-) \approx q^*(\zeta_i^+) - q^*(\zeta_i^-). \end{aligned} \tag{3.24}$$

More precisely, note (see also Figure 4) that for each jump, the landing point is closer to a knee of $\mathcal{S}$ than is the corresponding take-off point. We thus have $F'(u(\zeta_i^+)) > F'(u(\zeta_i^-))$ for each i. Since $q^*(\zeta_2^+) > q^*(\zeta_2^-)$ from (3.20) and (3.23), corresponding to the jump down, it therefore follows from (3.24) that $u^*(\zeta_2^+) > u^*(\zeta_2^-)$. On the other hand, since $q^*(\zeta_1^+) < q^*(\zeta_1^-)$ from (3.20) and (3.22), corresponding to the jump up, (3.24) does not allow us to analytically guarantee the direction of the jump in u^* at ζ_1. However, each jump in u^* is predicted to be in the same direction as the corresponding jump in q^* for $F'(u(\zeta_i^\pm))$ sufficiently small, and these values are certainly small in Figure 3(a), so we can at least predict that these directions will agree.

3.3. Numerical simulations of the pulse. In theory, (3.20)–(3.23), together with the exponential behavior of q^* between jumps as given by (3.18), characterize the function $u^*(\xi - \theta)$ for any fixed θ and, hence, fix the speed c_1 through (3.9). In this subsection, we consider some numerical simulations of traveling pulse solutions of (3.1). In the next subsection, we turn to some simulations that illustrate the properties of u^* and their use in estimating the range of stimulus speeds that can be tracked, based on (3.9).

As in the case of fronts, we perform simulations here on $x \in [-1, 1]$ with even boundary conditions, and we retain the same functions F and J used in subsection 2.3, but we now assume that each stimulus function is a hat-shaped pulse with $\varepsilon I(\xi) = I_0 H(-\xi - 0.8)H(\xi + 1)$ with $I_0 \in \{\pm 0.01, \pm 0.05\}$ for some choice of $c > 0$ and $\xi = x - ct$. Also, in (3.1) we choose $\beta = 0.25$ and $\kappa = 0.02$. The parameters used yield an unstimulated pulse speed of $c_0 \approx 1.25$. We activate the leftmost 5% of the domain with initial conditions $u(x, 0) = 0.7H(-x - 0.9)$ and initiate the stimulus

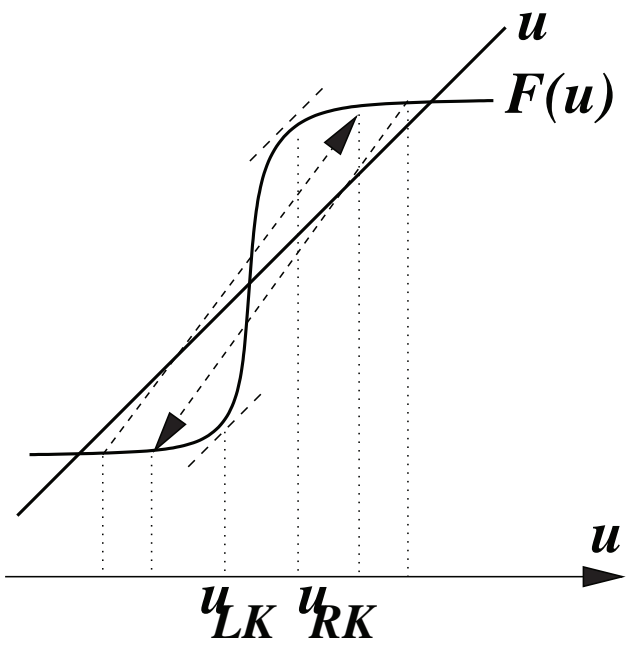

FIG. 4. *Illustration of $F'(u)$ at jump points. The knees of $\mathcal{S}$ occur at the values $u = u_{LK}$ and $u = u_{RK}$, where $F'(u) = 1$, as indicated by the corresponding dashed segments. The directions of the jumps up and down are illustrated by the dashed lines with arrows. The jump up shown here occurs in the direction of increasing u, from a point below u_{LK} to a point above, but closer to u_{RK}, leading to an increase in $F'(u)$ across the jump. The jump down occurs in the direction of decreasing u, from a point above u_{RK} to a point below, but closer to u_{LK}, also leading to an increase in $F'(u)$ across the jump.*

pulse with its leading edge at $x = -0.8$, slightly ahead of the activated region. With $I_0 = 0.05$ and a stimulus speed of $c = 1.8$, for example, the pulse that is initiated by the initial conditions appears to succeed in tracking closely behind the stimulus and propagating from left to right with the same speed as the stimulus pulse. This result is illustrated in Figure 5(a), where we plot $u(x,t) + 18\varepsilon I(x,t)$ to show the close tracking of the wave pulse to the stimulus pulse. With all the same conditions and a faster stimulus speed of $c = 2.0$, the simulated wave pulse fails to keep up with the faster stimulus pulse, as shown in Figure 5(b). Unlike for the case of fronts, stimulus-locked pulses also occur for stimulus speeds that are slower than the natural wave speed. A successful stimulus-locked pulse for $c = 1.2$ is shown in Figure 5(c), whereas a failure for $c = 1.1$ is shown in Figure 5(d).

For a negative (inhibitory) stimulus pulse with $I_0 = -0.05$ and all other conditions unchanged, successful stimulus-locked traveling pulses are shown in Figures 6(a) and (c) for $c = 1.3$ and $c = 0.85$, respectively. Failures to obtain stimulus-locked pulses are shown in Figure 6(b) and (d) with $c = 1.4$ and $c = 0.75$, respectively. In Figure 6, $u(x,t) - 22\varepsilon I(x,t)$ is plotted in each case to show the relation of the traveling pulse to the stimulus pulse.

As with fronts, we note that the successful stimulus-locked pulses in Figures 5–6 correspond to traveling pulses on the real line while the pulselike solutions that fail to lock to the stimulus do not represent true traveling pulse solutions on the real line but rather provide evidence that traveling pulse solutions do not exist for those values of c outside of the existence interval. Also, as in the case of fronts,

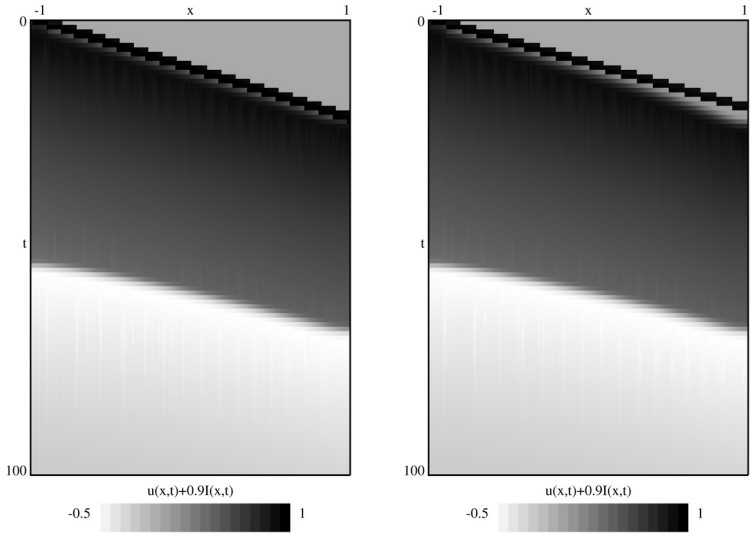

(a) c=1.8

(b) c=2.0

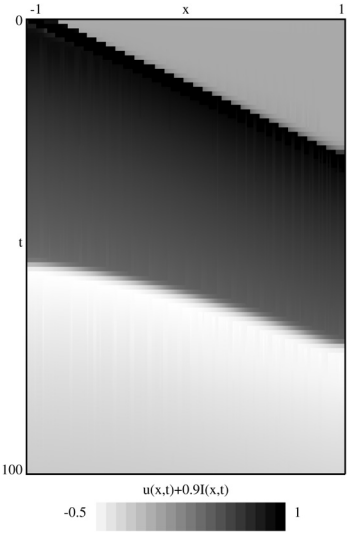

(c) c=1.2

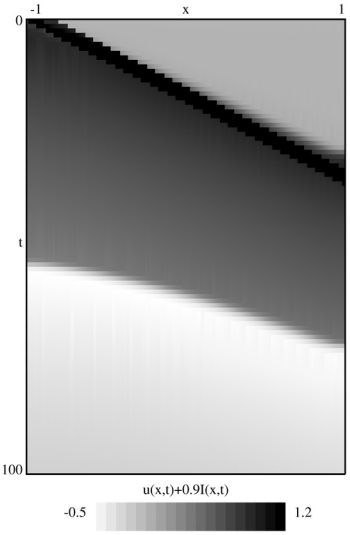

(d) c=1.1

FIG. 5. *Stimulus-locked traveling pulses with stimuli of positive amplitude.* (a), (c) *Successful and* (b), (d) *failed propagation with* $\varepsilon I(x,t) = 0.05H(-(x-ct)-0.8)H(x-ct+1)$ *for specified stimulus speeds. For these simulations,* $F(u) = 1/(1+\exp(-20u+5))$, $J(x) = 10\exp(-20|x|)$, $\beta = 0.25$, *and* $\kappa = 0.02$.

successful stimulus tracking occurs over larger intervals of speeds for stimuli that are sigmoidal approximations to the Heaviside function, with interval size growing as the slope of the sigmoid decreases. Unlike the case of fronts, we find that for a fixed I_0, pulses can track various stimuli with speeds that are slower or faster than the unstimulated speed, consistent with the idea that u^* is not sign-definite

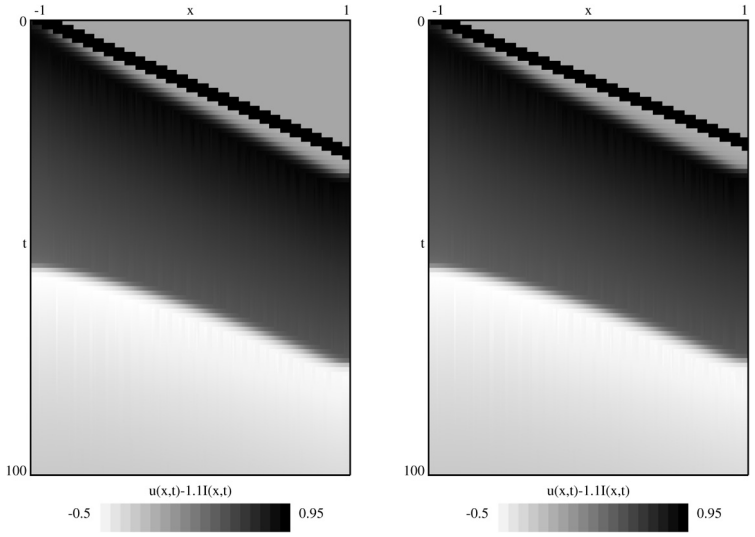

(a) c=1.3 (b) c=1.4

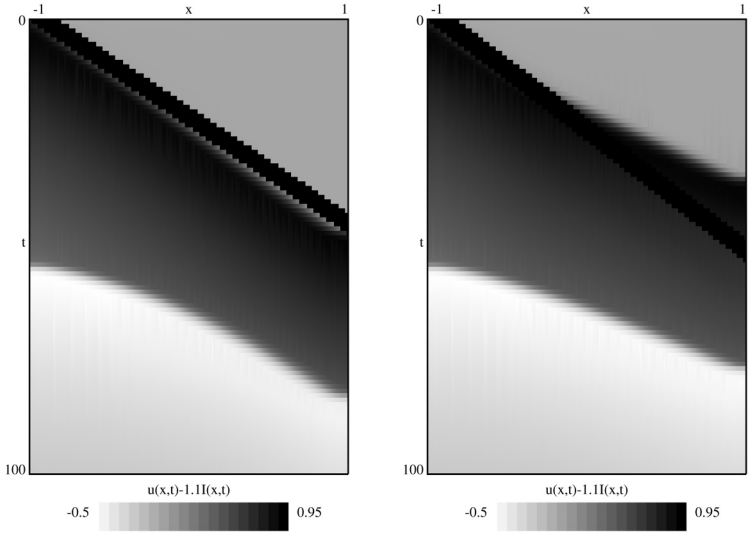

(c) c=0.85 (d) c=0.75

FIG. 6. *Stimulus-locked traveling pulses with stimuli of negative amplitude.* (a), (c) *Successful and* (b), (d) *failed propagation under the same conditions illustrated in Figure* 5*, except* $\varepsilon I(x,t) = -0.05H(-(x-ct)-0.8)H(x-ct+1)$.

in (3.9). It is difficult to judge by inspection just when successful stimulus tracking is or is not occurring in our simulations, particularly since we are restricted to a domain of finite size. It is apparent, however, that the interval about the natural wave speed for which stimulus-locked pulses exist when $I_0 = 0.05$ is approximately reflected about the natural wave speed when $I_0 = -0.05$, as shown in Figures 5

and 6. Furthermore, when the magnitude of I_0 decreases, say from 0.05 to 0.01, the interval of speeds for which stimulus-locked traveling pulses exist shrinks, and progressively better agreement between intervals for positive and negative I_0 emerges, again consistent with (3.9) and Remark 3.2.

3.4. Numerical approximations of the pulse speed. For the pulse equations (3.1), it is very difficult to compute the adjoint, and we do not know of a numerical method for doing it since we cannot really accurately compute the pulse with shooting. However, as in subsection 3.2, we can put the system on a large periodic domain of length L. The idea behind this step is that the resulting wave train will be similar to the solitary pulse if the distance between waves is sufficiently large such that the adaptation has time to wear off, and it is as if the pulse is moving into a resting medium each time it recurs. This approach has an additional advantage in that it allows us to make the stimulus move around the domain at some velocity c so that it becomes temporally periodic with period $T = L/c$ and frequency $\omega = c/L$. The result is that our system becomes like an intrinsic oscillator subject to weak periodic forcing. If L is large enough relative to c, then this system is a good approximation to the driving of a pulse with a traveling stimulus on an infinite domain. For example, we simulated a domain of length $L = 300$ and, without a stimulus, find a pulse solution with a temporal period of $T = 243$. The corresponding baseline pulse velocity $c_0 = 1.2345679$ (with frequency $\omega_0 = 0.004115$) is not too far from the front velocity of 1.3, which the pulse velocity on the infinite domain should approach as $\kappa \downarrow 0$, so we conclude that the domain length is reasonable for our approximation.

We next apply the following stimulus:

$$I_a(x,t) = I_0 \exp(-K(1 - \cos(x/L - \omega t))),$$

with $K = 100$. Figure 7(A) shows simulations of the pulse $u(x,t)$ together with the scaled stimulus $\varepsilon I_a(x,t)$, with $\varepsilon I_0 = 0.05$ and $F(u) = 1/(1+\exp(-20u+5))$ as previously, at a fixed spatial location for two different stimulus velocities c, one above and one below the natural frequency c_0. In these examples, for a velocity (frequency) faster (higher) than the natural one, the stimulus leads the pulse, but only by a very short time, as seen in the bottom of Figure 7(A). For a lower velocity, the stimulus lags the pulse, and the wave is still able to lock to the stimulus, as seen at the top of Figure 7(A).

We estimate the range of velocities over which tracking occurs by direct numerical simulation and by our analysis from subsection 3.1. First, we systematically vary c and numerically compute a solution to the full spatiotemporal wave model on the ring of length $L = 300$ for each fixed value, using $\varepsilon I_0 = 0.05$. For each, we calculate the timing difference between the arrival times of the stimulus and the pulse at a fixed spatial location on each of several cycles on which the stimulus and pulse pass through that location. If the pulse is tracking the stimulus, then the same time difference at this location should arise on each cycle. The results of these simulations are displayed in Figure 7(D). Although it is difficult to judge by eye, especially because delayed convergence may cause some differences across cycles for values where tracking occurs, we estimate roughly that tracking occurs over a range of velocities from $c_{min} = 1.23$ to $c_{max} = 1.66$. This means that c_1 must lie between $(c_{min} - c_0)/(\varepsilon I_0) \approx -0.1$ and $(c_{max} - c_0)/(\varepsilon I_0) \approx 8.5$. We observe that for a pulse to track a stimulus that is slower than the natural velocity, the stimulus velocity has to be quite close to the natural velocity, in agreement with what was found for the Heaviside case in earlier work [13].

According to the analysis in subsection 3.1, the equations for the values of c_1 such that tracking occurs for speeds $c = c_0 + \varepsilon c_1 + \dots$ are given by the Fredholm alternative

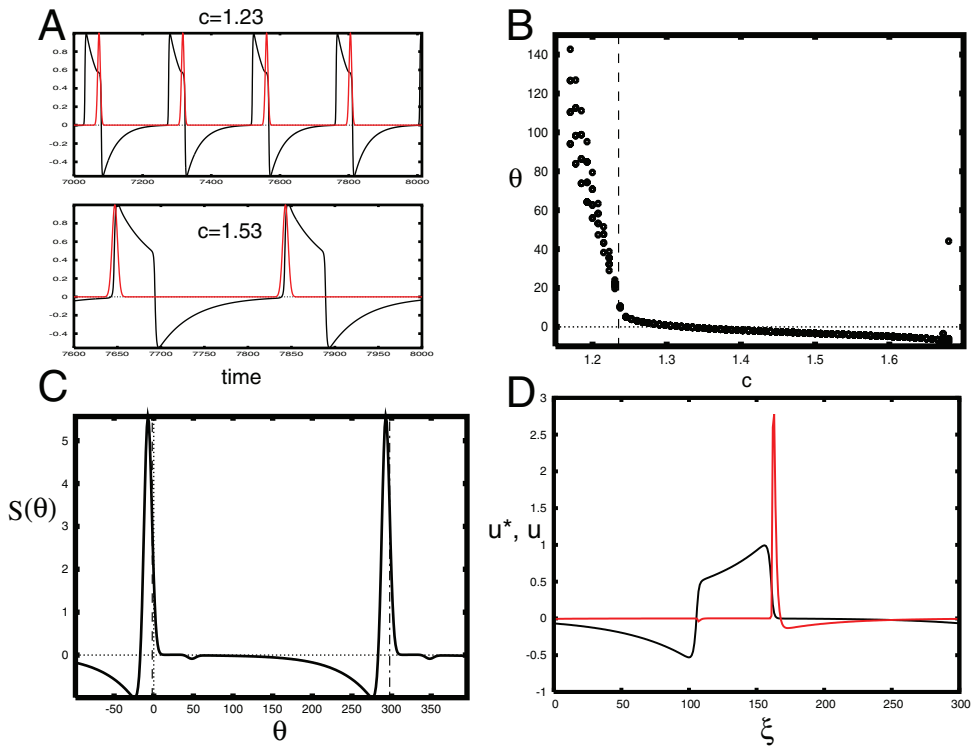

FIG. 7. *Numerical simulations for the pulse and its adjoint. Relevant parameter values are* $\varepsilon I_0 = 0.05, \beta = 0.25, \kappa = 0.02$, *with* $F(u) = 1/(1+\exp(-20u+5))$. (A) *Pulse component* u *(broad peaks) and scaled stimulus* εI_a *(narrow peaks) from* (3.1), *given as functions of time. The stimulus lags the pulse for* $c = 1.23 < c_0$ *and slightly leads the pulse for* $c = 1.53 > c_0$. (B) *Spatial lag* θ *between the stimulus and pulse as a function of stimulus speed* c *at a fixed spatial location* ($x = 0$). *The dashed line marks the baseline speed* c_0 *(a lag occurs here because presenting a stimulus at this speed does affect the velocity of the resulting pulse). Imperfect tracking can yield different* θ *values on different cycles, as seen for the smallest and largest* c *values here, although this can also occur due to transients before perfect tracking is achieved.* (C) *Numerically calculated* $S(\theta)$, *with dash-dotted lines at* $\theta = 0$ *and* $\theta = 300$, *the domain period.* (D) *Numerically calculated* $u(\xi)$ *(broad peak) and* $u^*(\xi)$ *(narrow peak) used to compute* $S(\theta)$.

expression (3.7), and on the periodic domain this becomes

$$-c_1 \int_0^L (u^*(\xi)u'(\xi) + q^*(\xi)q'(\xi))\, d\xi = \int_0^L I_a(\xi-\theta)u^*(\xi)\, d\xi.$$

With the normalization condition $\int_0^L (u^*(\xi)u'(\xi) + q^*(\xi)q'(\xi))\, d\xi = 1$ from (3.8), we obtain

$$c_1 = -\int_0^L I_a(\xi-\theta)u^*(\xi)\, d\xi := S(\theta). \tag{3.25}$$

We have used XPPAUT [8] to calculate the adjoint for the long periodic orbit at a certain location in space—say $x = 0$. This is the "timelike" adjoint; whereas (3.25) incorporates the spacelike adjoint, so we use a change of variables to evaluate the integrals in (3.25). The resulting $S(\theta)$ is shown in Figure 7(C), with corresponding

functions $u(\xi), u^*(\xi)$ used to compute $S(\theta)$, displayed in Figure 7(D). The maximum and minimum of $S(\theta)$ give us theoretical bounds on the range of c_1 for which there is a spatial translation θ at which tracking occurs.

To interpret these results, consider first the case of $\theta = 0$, or no lag. According to Figure 7(B), this should occur at about $c = 1.32$, or $c_1 \approx (c - c_0)/(\varepsilon I_0) \approx 1.71$. From Figure 7(C), $S(0) \approx 2.1$, showing a good agreement between theory (C) and direct simulation (B). Starting from $\theta = 0$, increases in θ yield decreases in $c_1 = S(\theta)$ in Figure7(C), until eventually, $S(\theta)$ goes negative, corresponding to stimuli that are slower than the baseline velocity c_0. This result also agrees with Figure 7(B), where we see speeds below 1.32 giving lags $\theta > 0$, with θ growing sharply larger as speeds become less than $c_0 \approx 1.235$, marked with the vertical dashed line in the Figure 7(B). Interestingly, the size of the first negative peak in $S(\theta)$, near $\theta = 50$, agrees with the numerically computed lower bound $c_1 = -0.1$. Thus, we conjecture that the part of $S(\theta)$ from that peak up to $\theta \approx 275$, including the large negative peak of $S(\theta)$, corresponds to waves that we do not observe numerically and are perhaps unstable.

Returning to $\theta = 0$, if we decrease θ, we enter a regime where the stimulus leads the pulse, and Figure 7(C) predicts increasing speeds $c_1 = S(\theta)$ up to a peak of about 5.5. This prediction matches up with the results in Figure 7(B) for $c > 1.32$, where θ becomes more negative as c increases. Although the predicted maximum c_1 from Figure 7(B) exceeds that predicted by Figure 7(C), the two agree qualitatively, and both predict that tracking with positive c_1 will involve only a very narrow range of lags θ. Finally, the θ values below the positive peak in $S(\theta)$ were not observed numerically and could correspond to unstable solutions.

We note that for negative stimulus pulses of equal amplitude, the graph of $S(\theta)$ gets reflected about the θ-axis, and the theoretical bounds for stimulus-locked pulse speeds should be reflected about the natural wave speed as noted in Remark 3.2. Our direct simulations analogous to those in Figure 7(B) for a negative pulse of equal magnitude are consistent with this finding. Also, the existence intervals for stimulus-locked pulse speeds obtained by the direct simulations on the ring in this section are consistent with those on $[-1, 1]$ suggested by Figures 5–6.

Our numerical calculations have yielded an example of $u^*(\xi)$, as shown in Figure 7(D). To conclude this section, we recall that we have done calculations based on periodic solutions of system (3.12) to derive analytical expressions relating to the adjoint solution, and we can now compare our numerical and analytical results. Figure 8 shows $u^*(\xi), q^*(\xi)$ for our numerically computed adjoint solution; $u^*(\xi)$ is the same function shown in Figure 7(D). The analytical calculations in subsection 3.2, based on (3.20)–(3.24), suggested that (1) q^* would decrease at the front and increase at the back, (2) the jumps in u^* would be in the same direction as these jumps in q^*, (3) the jumps in u^* and q^* would be of comparable magnitude, and (4) the δ-function excursions in u^* would be in the opposite directions to these jumps. In Figure 8, the front occurs near $\xi = 170$ and the back near $\xi = 120$, where a small deflection in the curves occurs. To a great extent, the predictions of the analysis match the numerical results. Note in particular that, while the δ-excursion of u^* at the front is in the positive direction, the net change in u^* across the front is negative, as is the jump in q^*. The only possible discrepancies are that we cannot resolve the direction of the jump in u^* at the back, since it is so small and the δ-excursion cannot be cleanly distinguished from the jump away from the singular limit, and the magnitude of the jump in u^* is significantly smaller than the jump in q^* at the front, although this may also relate to effects of the δ-excursion away from the singular limit.

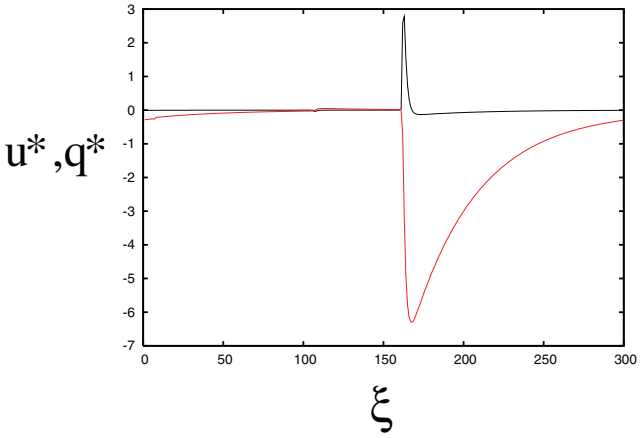

FIG. 8. *Numerically computed adjoint solution components $u^*(\xi)$ (trace with narrow peak) and $q^*(\xi)$ (trace with broad valley). Parameters and functions are as in Figure 7. The back occurs near $\xi = 120$, where the δ-function excursion in u^* is downward and q^* exhibits a positive jump, and the front occurs near $\xi = 170$, where the δ-function excursion in u^* is upward and both u^* and q^* exhibit negative jumps.*

4. Conclusions. In this work, we have considered the existence of traveling solutions in continuum neuronal models that include a propagating applied stimulus $\varepsilon I(x,t) = \varepsilon I(x - ct)$, where the amplitude parameter ε is small. We work with two forms of neuronal models, one lacking adaptation that yields traveling front solutions and another with adaptation that supports traveling pulse solutions. Past work by Bressloff et al. [2] and Folias and Bressloff [12, 13] analyzed traveling solutions in stimulated neuronal media with Heaviside firing rate functions. Papers by Ermentrout and McLeod [11] and Pinto and Ermentrout [20] considered the existence of traveling front and pulse solutions, respectively, in related models with more general, smooth firing rate functions, in the absence of spatiotemporally dependent applied stimulation. The current paper brings together these research directions, allowing for smooth firing rate functions in the stimulated case.

Our analysis shows that the Fredholm alternative can be used to leverage the existence of a traveling solution in a model lacking stimulation to ascertain the existence of a related, stimulus-locked traveling solution when a small amplitude stimulus is applied. Similar methods were also used by previous authors in the study of wave propagation in inhomogeneous media for a bistable equation [16] and for neural field equations [1, 17], as well as to study front bifurcations in neural fields with adaptation [3]. The range of speeds over which a solution exists, corresponding to successful tracking of the stimulus, can be estimated using this approach and depends on the form of the stimulus, although a general upper bound that does not depend strongly on this form can be derived in the traveling front case. This range of speeds also depends on the properties of a solution to an adjoint equation. We were not able to fully characterize the relevant adjoint solutions, but we do provide theoretical and numerical results that clarify some of their properties as well as numerical examples illustrating the intervals of speeds over which waves successfully track propagating stimuli and the success of the analytical estimates. Interestingly, the analysis and simulations show that the nature of these intervals differs between the case of a traveling front stimulus in a model lacking neuronal adaptation and the case of a traveling pulse stimulus in

a model including adaptation. In particular, in the case with adaptation, a stimulus of positive amplitude can induce a traveling pulse with speed slower than that of the unstimulated pulse, while positive amplitude stimuli always speed fronts up in the absence of adaptation.

5. Appendix. Here, we extract from Theorem A.1 of [15] the specific quantities used to compute the expressions in (3.20) and (3.21) and present a brief summary of the corresponding calculations. For a more complete statement and discussion of this theorem, see [15].

The vector field for the slow q equation is given by $(\beta q - u)/c$. Using $u = g_\alpha(q), \alpha \in \{L, R\}$, to denote the solutions of $q = F(u) - u$ as previously, we obtain the slow equation $\dot{q} = (\beta q - g_\alpha(q))/c$ on the slow manifold $\mathcal{S}$. From this expression, the corresponding adjoint equation is $\dot{q}^* = -(\beta/c)q^* + (1/c)g'_\alpha(q)q^*$, as given in (3.18). Note that this is the same equation as we obtain from the system (3.15) and (3.16), together with (3.17), in the singular limit $\kappa \to 0$.

To compute the jumps in the solution of (3.18), we need to find the left eigenvector w_j of the Jacobian matrix of the fast subsystem of (3.12) to which the jump take-offs are tangent. The relevant matrix is given by

$$J = \begin{bmatrix} 1/c & -1/c & 0 \\ 0 & 0 & 1 \\ -F'(u) & 1 & 0 \end{bmatrix}.$$

If we let λ denote any eigenvalue of J, then a corresponding left eigenvector is given by

$$w_j = [c - c\lambda^2 \;\; \lambda \;\; 1]. \tag{5.1}$$

We shall see below that we will get the same jump directions and magnitudes no matter what nonzero constant multiple of w_j we use to compute them.

Remark 5.1. Note that the characteristic equation of J is $\lambda^3 - \lambda^2/c - \lambda + (1/c)(1 - F'(u)) = 0$ such that $\lambda = 1$ is an eigenvalue if and only if $F'(u) = 0$. If $F'(u) = 0$, then the eigenvalues of J are $\lambda = \pm 1, 1/c$. In fact, it can be shown that the eigenvalue corresponding to the left eigenvector governing the jump direction, in the limit $F'(u) \to 0$, tends to $\lambda = 1$. If this limit is reached, then the jump calculations break down, since $w_j = [0 \;\; 1 \;\; 1]$ results, but the only q^* dependence appears in the u^* equation.

Besides w_j, the jump calculations also use the vector f_q, corresponding to the vector of partial derivatives of the fast subsystem vector field with respect to q, given by $f_q = [1/c \;\; 0 \;\; 0]^T$. This quantity, (5.1), and (3.19) can be substituted into the following formula:

$$c_j := w_j^T \left(\frac{q^*(\zeta_j^-)g(b_j) - 1}{w_j f_q g(b_j)} \right) = \begin{bmatrix} c - c\lambda^2 \\ \lambda \\ 1 \end{bmatrix} \left(\frac{\frac{G(b_j)}{G(a_j)} - 1}{[c - c\lambda^2 \;\; \lambda \;\; 1] \begin{bmatrix} 1/c \\ 0 \\ 0 \end{bmatrix} \left[\frac{(\beta q - g_\alpha(q))}{c} \right]\Big|_{b_j}} \right)$$

$$= c \begin{bmatrix} c - c\lambda^2 \\ \lambda \\ 1 \end{bmatrix} \left(\frac{G(b_j) - G(a_j)}{(1 - \lambda^2)G(a_j)G(b_j)} \right), \tag{5.2}$$

where $G(x) = (\beta q - g_\alpha(q))|_{(u,q,w,z)=x}$ as previously. Note that multiplication of w_j by a nonzero constant does not change this result, as claimed above.

Now, Theorem A.1 of [15] specifies that

$$q^*(\zeta_j^+) = q^*(\zeta_j^-) - f_q^T c_j = q^*(\zeta_j^-) - c\left(\frac{G(b_j) - G(a_j)}{G(a_j)G(b_j)}\right). \tag{5.3}$$

If we set $y^* = [u^* \quad w^* \quad z^*]^T$, then the theorem also gives $y^*(\zeta) = -(D_y g(\zeta) D_y f(\zeta)^{-1})^T q^*(\zeta)$ for $\zeta \neq \zeta_j$, where D_y denotes differentiation with respect to the fast variables (u, w, z). At the jump points ζ_j, $y^*(\zeta)$ behaves as a δ-function, in the sense that

$$\int_{\zeta_j^-}^{\zeta_j^+} \dot{q}^*(\zeta) d\zeta = -\int_{\zeta_j^-}^{\zeta_j^+} f_q^T y^*(\zeta) d\eta. \tag{5.4}$$

From (5.3), the integral on the left-hand side of (5.4) evaluates to $-f_q^T c_j$ such that (3.21) results from formula (5.2).

REFERENCES

[1] P. C. Bressloff, *Traveling fronts and wave propagation failure in an inhomogeneous neural network*, Physica D, 155 (2001), pp. 83–100.

[2] P. C. Bressloff, S. Folias, A. Pratt, and Y. Li, *Oscillatory waves in inhomogeneous neural media*, Phys. Rev. Lett., 91 (2003), 178101.

[3] P. C. Bressloff and S. E. Folias, *Front bifurcations in an excitatory neural network*, SIAM J. Appl. Math., 65 (2004), pp. 131–151.

[4] R. G. Casten, H. Cohen, and P. A. Lagerstrom, *Perturbation analysis of an approximation to the Hodgkin-Huxley theory*, Quart. Appl. Math., 32 (1975), pp. 365–402.

[5] R. D. Chervin, P. A. Pierce, and B. W. Connors, *Periodicity and directionality in the propagation of epileptiform discharges across neocortex*, J. Neurophysiol., 60 (1988), pp. 1695–1713.

[6] B. W. Connors, D. J. Pinto, and A. E. Telfeian, *Local pathways of seizure propagation in neocortex*, Int. Rev. Neurobiol., 45 (2001), pp. 527–546.

[7] S. Coombes, *Waves, bumps, and patterns in neural field theories*, Biol. Cybernet, 93 (2005), pp. 91–108.

[8] B. Ermentrout, *Simulating, Analyzing, and Animating Dynamical Systems: A Guide to XPPAUT for Researchers and Students*, SIAM, Philadelphia, 2002.

[9] G. Ermentrout, *Neural nets as spatio-temporal pattern forming systems*, Rep. Progr. Phys., 61 (1998), pp. 353–430.

[10] G. B. Ermentrout and D. Kleinfeld, *Traveling electrical waves in cortex: Insights from phase dynamics and speculation on a computational role*, Neuron, 29 (2001), pp. 33–44.

[11] G. B. Ermentrout and J. B. McLeod, *Existence and uniqueness of travelling waves for a neural network*, Proc. Roy. Soc. Edinburgh Sect. A, 123 (1993), pp. 461–478.

[12] S. E. Folias and P. C. Bressloff, *Breathing pulses in an excitatory neural network*, SIAM J. Appl. Dyn. Syst., 3 (2004), pp. 378–407.

[13] S. E. Folias and P. C. Bressloff, *Stimulus-locked traveling waves and breathers in an excitatory neural network*, SIAM J. Appl. Math., 65 (2005), pp. 2067–2092.

[14] D. Golomb and Y. Amitai, *Propagating neuronal discharges in neocortical slices: Computational and experimental study*, J. Neurophysiol., 78 (1997), pp. 1199–1211.

[15] E. M. Izhikevich, *Phase equations for relaxation oscillators*, SIAM J. Appl. Math., 60 (2000), pp. 1789–1804.

[16] J. P. Keener, *Homogenization and propagation in the bistable equation*, Phys. D, 136 (2000), pp. 1–17.

[17] Z. P. Kilpatrick, S. E. Folias, and P. C. Bressloff, *Traveling pulses and wave propagation failure in inhomogeneous neural media*, SIAM J. Appl. Dyn. Syst., 7 (2008), pp. 161–185.

[18] K. Kishimoto and S. Amari, *Existence and stability of local excitations in homogeneous neural fields*, J. Math. Biol., 7 (1979), pp. 303–318.

[19] E. P. Krisner, *The link between integral equations and higher order ODEs*, J. Math. Anal. Appl., 291 (2004), pp. 165–179.

[20] D. J. Pinto and G. B. Ermentrout, *Spatially structured activity in synaptically coupled neuronal networks:* I. *Traveling fronts and pulses*, SIAM J. Appl. Math., 62 (2001), pp. 206–225.

[21] D. J. Pinto, S. L. Patrick, W. C. Huang, and B. W. Connors, *Initiation, propagation, and termination of epileptiform activity in rodent neocortex in vitro involve distinct mechanisms*, J. Neurosci., 25 (2005), pp. 8131–8140.
[22] K. A. Richardson, S. J. Schiff, and B. J. Gluckman, *Control of traveling waves in the mammalian cortex*, Phys. Rev. Lett., 94 (2005), 028103.
[23] K. Takagaki, C. Zhang, J. Y. Wu, and M. T. Lippert, *Crossmodal propagation of sensory-evoked and spontaneous activity in the rat neocortex*, Neurosci. Lett., 431 (2008), pp. 191–196.
[24] J. Y. Wu, X. Huang, and C. Zhang, *Propagating waves of activity in the neocortex: What they are, what they do*, Neuroscientist, 14 (2008), pp. 487–502.
[25] J. Y. Xu, *private communication*, Georgetown University, 2009.
[26] W. Xu, X. Huang, K. Takagaki, and J. Y. Wu, *Compression and reflection of visually evoked cortical waves*, Neuron, 55 (2007), pp. 119–129.